formation of a localized horizontal shear band S at the top or bottom part of the granular media (D1 in Fig. 4).

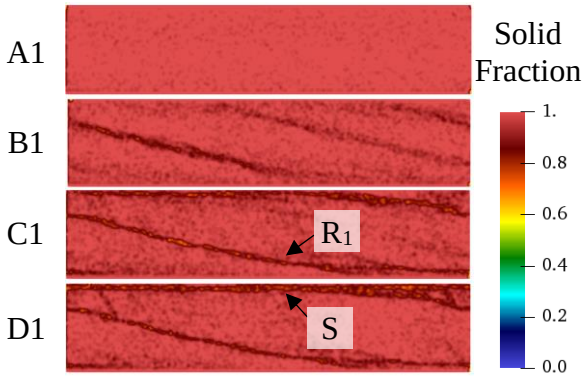

Fig. 4. Solid fraction as a function of a slip distance (mm) letter from figure 3, L_{10}.

3.2 Influence of inter-particle friction

Numerical experiments are difficult to calibrate, as input data injected in the model are poorly documented in real granular media (i.e. inter-particle friction). A change in inter-particle friction coefficient from 0.3 to 0.6 can yield significant differences in friction peak values (Fig. 5 (a)) (0.9 vs 1.3 for L_{10}). But both numerical experiments tend to the same averaged friction at steady state ($\mu_{ss} = 0.42$). A modification in inter-particle friction also changes the main orientation of Riedel shear bands (≈16° from the horizontal shear direction with $\mu_i = 0.6$).

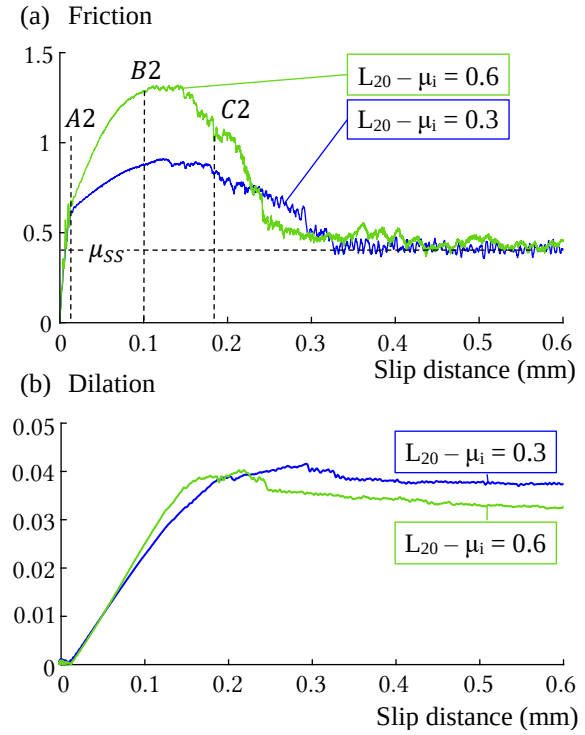

Fig. 5. (a) Friction coefficient as a function of the slip distance (mm) for different inter-particle friction ($\mu_i = 0.3$ & 0.6), for L20 (the same friction peak difference is observed for the other lengths of models). (b) Dilation as a function of the slip distance (mm) for the same cases.

Increasing inter-particle friction also seems to increase the number of Riedel bands formed at the beginning of friction peak (B2 in Fig. 5 & Fig. 6) and within the decreasing friction part (C2 in Fig. 6). This increase results in reducing the distance average d between Riedel bands (Fig. 6). Higher angle Riedel bands (≈45° from the horizontal shear direction) are also more pronounced with higher friction, (at C2 in Fig. 7).

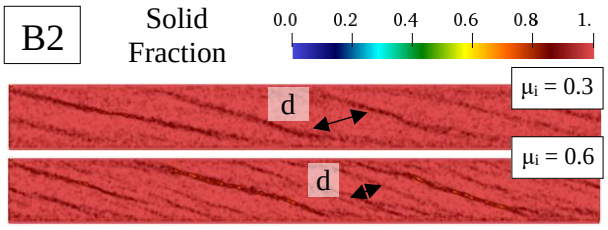

Fig. 6. Solid fraction at slip distance B2 for two different inter-particle frictions ($\mu_i = 0.3$ & 0.6), L_{20}, letter from Fig. 5.

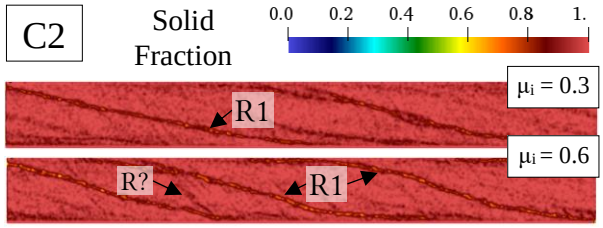

Fig. 7. Solid fraction at slip distance C2 for two different inter-particle frictions ($\mu_i = 0.3$ & 0.6), L_{20}, letter from Fig. 5.

The two Riedel bands described as low-angle (R1) and high angle (R2) do not have the same growing pattern. They both depend on porosity-weakening and strain-rate-weakening mechanisms [9]. Initial state of porosity is not modified here, but inter-particle friction plays a role on the rheology of the granular media, as it changes the contact between every polygonal cell. It may explain why high-angle Riedel bands are more pronounced with higher friction. The increasing number of Riedel bands with inter-particle friction can be explained with contact mechanics [10]. For the peak phase, when μ_i is low, slip may occur between polygonal cells, and particles are mobilized within the shear zone, with minimal dilation. With a higher μ_i, sliding is partly inhibited and particles tend to separate leading to higher dilations, and thus in our case, higher number of Riedel bands (i.e. dilation in specific direction). However, at the end of friction peak, Riedel bands reduce into a more stable behaviour and total dilation tends to be higher for the case with lower friction.

As shown in Fig. 5, an interparticle friction coefficient of 0.6 also leads to a more sudden post-peak weakening, which is prone to switch the fault behaviour from a ductile aseismic response to a brittle seismic slip, depending on the stiffness of the surrounding medium.

4 Conclusion

Changing the length of the fault gouge sample does not inhibit the formation of shear bands but it modifies the rate of friction weakening with the slip displacement. An increase of inter-particle friction seems to influence shear bands formation with two main consequences. The

orientation angle of Riedel bands from the horizontal slip displacement increases with the inter-particle friction (typical results from Mohr-Coulomb theory). Then, low-angle Riedel bands are mostly observed and their number increases with friction.

On-going studies are dedicated to mixing polygonal cells with angular grains in order to represent granitic particles with a cement (i.e. polygonal cells) between them. Different results are expected in terms of Riedel patterns as intern structure will be less homogeneous. A modification of matrix thickness could also influence the rheology of the fault.

References

[1] Y. Berthier, *Experimental evidence for friction and wear modelling*. Wear **139**, 77 (1990)

[2] P.A. Cundall, O.D.L. Strack, *A discrete numerical model for granular assemblies*, Geotech. **29**, 47 (1979)

[3] J.K. Morgan, M.S. Boettcher, *Numerical simulations of granular shear zones using the distinct element method: 1. Shear zone kinematics and the micromechanics of localization*, J. Geophys. Res. Solid Earth **104**, 2703 (1999)

[4] B. Ferdowsi, M. Griffa, R.A. Guyer, P.A. Johnson, C. Marone, J. Carmeliet, *Three-dimensional discrete element modeling of triggered slip in sheared granular media*, Phys. Rev. E **89**, 1 (2014)

[5] G. Mollon, *A multibody meshfree strategy for the simulation of highly deformable granular materials*, Int. J. Numer. Methods Eng. **108**, 1477 (2016)

[6] N. Casas, G. Mollon, A. Daouadji, *Cohesion and Initial Porosity of Granular Fault Gouges control the Breakdown Energy and the Friction Law at the Onset of Sliding*, ESSOAR (in prep)

[7] J.S. Tchalenko, *Similarities between shear zones of different magnitudes*, Geol. Soc. Am. Bull. **81**, 1625 (1970)

[8] Y. Katz, R. Weinberger, A. Aydin, *Geometry and kinematic evolution of Riedel shear structures, Capitol Reef National Park, Utah*, J. Struct. Geol. **26**, 491 (2004)

[9] R.F. Katz, M. Spiegelman, B. Holtzman, *The dynamics of melt and shear localization in partially molten aggregates*, Nature **442**, 2 (2006)

[10] J.K. Morgan, *Numerical simulations of granular shear zones using the distinct element method: 2. Effects of particle size distribution and interparticle friction on mechanical behavior*, J. Geophys. Res. Solid Earth **104**, 2721 (1999)